HEALTH AND MEDICINE

Wireless, skin-interfaced sensors for compression therapy

Yoonseok Park[1,2]*, Kyeongha Kwon[3]*, Sung Soo Kwak[1,2,4]*, Da Som Yang[1,2]*, Jean Won Kwak[1,2,5]*, Haiwen Luan[1,2,5,6], Ted S. Chung[1,2,7], Keum San Chun[8], Jong Uk Kim[1,9], Hokyung Jang[10], Hanjun Ryu[1,2], Hyoyong Jeong[1,2], Sang Min Won[11], Youn J. Kang[1,2], Michael Zhang[2], David Pontes[2], Brianna R. Kampmeier[2], Seon Hee Seo[1,12], Jeffrey Zhao[13], Inhwa Jung[14], Yonggang Huang[1,2,5,6,15], Shuai Xu[1,2,13†], John A. Rogers[1,2,5,7,14,16†]

Therapeutic compression garments (TCGs) are key tools for the management of a wide range of vascular lower extremity conditions. Proper use of TCGs involves application of a minimum and consistent pressure across the lower extremities for extended periods of time. Slight changes in the characteristics of the fabric and the mechanical properties of the tissues lead to requirements for frequent measurements and corresponding adjustments of the applied pressure. Existing sensors are not sufficiently small, thin, or flexible for practical use in this context, and they also demand cumbersome, hard-wired interfaces for data acquisition. Here, we introduce a flexible, wireless monitoring system for tracking both temperature and pressure at the interface between the skin and the TCGs. Detailed studies of the materials and engineering aspects of these devices, together with clinical pilot trials on a range of patients with different pathologies, establish the technical foundations and measurement capabilities.

INTRODUCTION

Compression therapy is the standard of care for a wide range of lower extremity conditions, including venous and lymphatic insufficiencies, lymphedema, venous stasis dermatitis, varicosities, and deep vein thrombosis (*1*). Compression therapy is particularly important in the treatment of venous leg ulcers (VLUs). VLUs remain the most common ulcerative wounds of the lower extremities, affecting more than 500,000 elderly patients at a cost of greater than $2 billion yearly (*2*). While cellular-based strategies such as the allogeneic matrix (*3*, *4*) and living cell–based constructs (*5*) have been developed to address this condition, they remain prohibitively expensive and offer unclear comparative efficacy (*6*). Hence, there is a lack of clinical consensus on their optimal use and practical utility (*7*). By contrast, compression therapy that delivers controlled pressures across the surface of the skin yields complete healing rates of up to 90%, when used regularly over 6 months (*8*, *9*). Therapeutic compression garments (TCGs) include both inelastic bandages (IBs), which can be adjusted for pressure strength, and graduated compression stockings (GCSs), which are static in pressure delivery once applied. This latter approach represents the most common modality given its ease of use and widespread availability (*1*). Consistent use after healing reduces the risk of a recurrent VLU by 2 to 20 times (*10*), as the standard of care for VLU therapy (*11*). A key practical challenge is in the design of TCGs that apply a constant, consistent pressure of ~40 mmHg across the leg for continuous use. Both IB and GCS suffer from a key limitation; when applied, there is a lack of technologies that are able to provide confirmatory evidence of sufficient interface pressure for clinical benefit.

In this respect, capabilities for actively and continuously monitoring the pressure have the potential to allow for precise control and optimized treatment. Several reports describe the use of various types of thin, soft pressure sensors for such purposes, including piezoresistive-type commercial sensors (*12*–*15*). The sizes of these devices, their thicknesses, and their high-modulus mechanical properties represent fundamental barriers to achieving accurate measurements and to providing a comfortable, irritation-free interface to the surface of the skin. Furthermore, the relatively large dimensions (over 10 mm in many cases) of these sensors lead to responses that depend not only on pressure but also on bending in a way that can be difficult or impossible to separate during practical use. The most widely accepted standard relies on an air bladder (PicoPress) as a manometry-based, universal method to measure applied interface pressure on the legs in the clinic. Cumbersome external hardware and wired interfaces present obstacles for use in the home. These aspects also prevent continuous monitoring during daily activities or during sleep. Features in an ideal alternative technology include (i) miniaturized dimensions (thickness as well as length and width) and soft, flexible, lightweight construction; (ii) high measurement accuracy and repeatability; (iii) applicability to

[1]Querrey Simpson Institute for Bioelectronics, Northwestern University, Evanston, IL 60208, USA. [2]Center for Bio-Integrated Electronics, Northwestern University, Evanston, IL 60208, USA. [3]School of Electrical Engineering, Korea Advanced Institute of Science and Technology, Daejeon 34141, Republic of Korea. [4]School of Advanced Materials Science and Engineering, Sungkyunkwan University (SKKU), Suwon 16419, Republic of Korea. [5]Department of Mechanical Engineering, Northwestern University, Evanston, IL 60208, USA. [6]Department of Civil and Environmental Engineering, Northwestern University, Evanston, IL 60208, USA. [7]Department of Biomedical Engineering, Northwestern University, Evanston, IL 60208, USA. [8]Electrical and Computer Engineering, The University of Texas at Austin, Austin, TX 78712, USA. [9]School of Chemical Engineering, Sungkyunkwan University (SKKU), Suwon 16419, Republic of Korea. [10]Department of Electrical and Computer Engineering, University of Wisconsin-Madison, Madison, WI 53706, USA. [11]Department of Electrical and Computer Engineering, Sungkyunkwan University (SKKU), Suwon 16419, Republic of Korea. [12]Nano Hybrid Technology Research Center, Creative and Fundamental Research Division, Korea Electrotechnology Research Institute (KERI), Changwon 51543, Republic of Korea. [13]Department of Dermatology, Feinberg School of Medicine, Northwestern University, Chicago, IL 60611, USA. [14]Department of Mechanical Engineering, Kyung Hee University, Yongin 17104, Republic of Korea. [15]Department of Materials Science and Engineering, Northwestern University, Evanston, IL 60208, USA. [16]Department of Neurological Surgery, Feinberg School of Medicine, Northwestern University, Chicago, IL 60611, USA.
*These authors contributed equally to this work.
†Corresponding author. Email: stevexu@northwestern.edu (S.X); jrogers@northwestern.edu (J.A.R.)

curved surfaces without adverse or confounding effects of bending; and (iv) wireless communication capabilities compatible with standard consumer devices (smartphones, tablets, etc.). Additional function in temperature sensing is also desirable, to monitor the progress of wound healing and to diagnose the effect of treatment by measuring skin temperature adjacent to the ulcers during their recovery.

This paper reports advances in materials science and biomedical engineering that serve as the basis for a technology with all of these attributes, in the form of a millimeter-scale soft, thin, and flexible pressure and temperature-sensing system with wireless communication capabilities for monitoring the interface between the skin and the compression garment, continuously and in nearly any environment with minimal burden on the user. Several key characteristics enhance patient care in this context. First, clinicians can use this technology as a point of care diagnostic tool to ensure that a GCS applies the minimum prescribed pressure necessary to promote healing (*16*). Second, clinicians and patients alike can exploit this device for continuous monitoring in the home setting, outside of hospital or laboratory environments. This mode of operation is important because lower limbs typically exhibit improvements in edema within 24 hours after donning a GCS, thereby leading to a decrease in the original target pressure by 37 to 48% (*17*). Thus, garments must be loosened and tightened depending on patient use patterns to maintain an appropriate target pressure but to avoid excessive, ischemia-inducing levels of compression. Third, wearable platforms that support pressure and temperature sensing can supply compliance information to clinicians, via periodic sampling of these quantities. This feature is important because consistent wear by patients with both GCS and IBs is highly variable (*18*).

RESULTS

An exploded view illustration of the system (Fig. 1A) highlights various aspects of the constituent layers and components: silicone encapsulation layers, a coin cell battery (CR1220), a three-dimensional (3D) pressure sensor (R_P), a temperature sensor (R_T), and electronics. The substrate is a thin, flexible copper-clad polyimide (PI) film (AP8535R, Pyralux) processed with a laser cutting tool (ProtoLaser U4, LPKF) to yield conductive traces that interconnect a Bluetooth low energy (BLE) system on a chip (SoC) and Wheatstone bridge circuits configured with sensors. The thin, flexible, and lightweight construction avoids irritation at the skin surface, yielding a nearly imperceptible interface with a donned GCS. Figure 1B presents circuit and functional block diagrams of the operation and the wireless interface to a smartphone. Wheatstone bridge circuits that include resistive sensors and reference resistors (R, R_{P0}, and R_{T0}; 10, 2.1, and 9.75 kilohms, respectively) convert resistive measurements of pressure and temperature (R_P and R_T) into corresponding voltages. Subsequent amplifiers (AMPs) compare the bridge voltages to a reference voltage (V_{REF}; 1.65 V) and amplify the differences with the fixed gain of 6. R_{P0} and R_{T0} denote the base resistances of the pressure and temperature sensors, respectively, such that the voltage outputs of the AMPs (V_P and V_T) are 0 V at these conditions. A central processing unit activates a general purpose input/output (GPIO) pin to supply a voltage (VDD) to the analog front-end circuits when the analog-to-digital converter (ADC) samples the AMP outputs and transmits ADC-sampled data via a BLE radio to a user interface (smartphone). The system performs pressure/temperature measurements at a 100-Hz sampling rate and transmits an averaged pressure/temperature value every 0.25 s (4 Hz) to the user interface for this experiment. For transmission rates of 0.1 Hz (every 10 s), the replaceable battery shown here (CR 1220; 3 V, 37 mA·h) has an expected lifetime of 120 days.

Figure 1C shows pictures of an encapsulated SCV (biomedical sensor for monitoring compression therapy of VLUs) adhered to the bare surface of a leg of a healthy volunteer without (left) and with (right) a compression stocking. The width, length, thickness, and weight of the complete system are 20 mm (W), 35 mm (L), 2.5 mm (T), and 3 mg, respectively. A biomedical adhesive (3M 1524) ensures robust bonding to the skin. Stable operation is possible for bending angles much larger (up to 60°; Fig. 1, D and E) than typical values (>5°) during application on the leg. For bending to 60°, the top and bottom copper traces experience strains less than the yield thresholds of the metal (0.3%).

A key component of this system is a 3D structure instrumented with inorganic strain gauges as the basis for a soft pressure sensor, tailored to meet the performance requirements of the present application. Many alternative concepts for pressure sensors can be found in the recent literature (*19*). Most rely on organic polymers and/or surface relief features in conductive composites (*20*–*22*), porous materials (*23*, *24*), and architected geometries (*25*–*27*); others exploit microchannels and liquid metal (*23*, *28*, *29*). Although these and other options can be considered in the present context, the devices outlined here are attractive because they can be tailored in a systematic manner, guided by computational modeling, for desired behaviors with materials and fabrication processes that are well aligned with commercial practice in consumer electronics. The resulting sensors can be integrated directly onto flexible printed circuit boards (FPCBs) in miniaturized geometries (diameter, 3 mm; height, 500 μm).

The fabrication exploits techniques of mechanically guided assembly (*30*, *31*) applied to a planar, lithographically fabricated multilayer stack (2D precursor; Fig. 2A and fig. S1) that includes (i) a layer of PI (PI2545, HD MicroSystems; 10 μm in thickness) on the bottom, (ii) a network of interconnects and four precision, resistive strain gauges connected in series (a gold trace in a serpentine geometry; width, 3 μm; thickness, 50 nm; resistance, 2.1 kilohm; fig. S2, A and B), and (iii) a layer of PI (1 μm in thickness) on top. The four gold traces located on the four legs of the resulting table-shaped 3D structure enable highly sensitive measurements of strain, with an elastic response across the full range of pressures (0 to 60 mmHg) of interest for the application discussed here [computed by finite element analysis (FEA); Fig. 2D]. Related work on similar 3D pressure sensors includes multimodal sensing using silicon nanomembranes (*32*) and metal traces (*33*) with operating ranges of 5 to 30 kPa (~37.5 to ~225 mmHg) and up to 350 kPa (~2625 mmHg), respectively. The alternative designs presented here achieve accurate measurements across the range of low pressures needed for GCS (0 to 60 mmHg). For example, the top and bottom layers of PI have different thicknesses, to place the metal at a location that lies outside of the neutral plane and, accordingly, leads to an increase in resistivity, through the piezoresistive effect, with increasing pressure due to out-of-plane bending. A low-modulus (E = 69 kPa) silicone material (Ecoflex 00-30, Smooth-On) encapsulates this 3D structure in a molded shape (diameter, 3 mm; height, 500 μm). This entire construct compresses by ~2.5 and ~12% under applied pressures of 30 and 150 mmHg, respectively. Optical images and FEA results for the 2D precursors and corresponding 3D structures show good

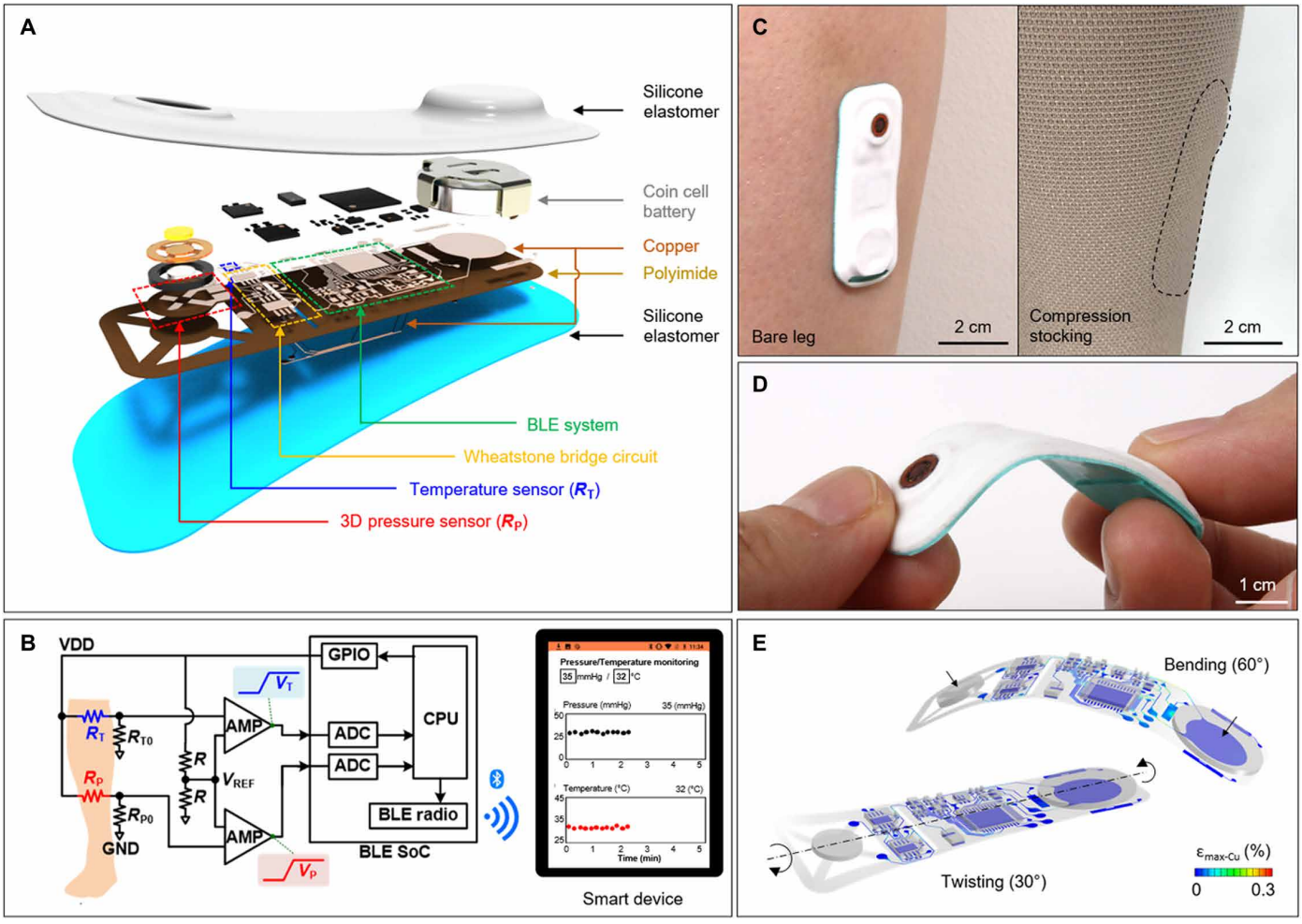

Fig. 1. Design and characterization of a wireless device for monitoring the treatment of VLUs with compression stockings. (**A**) Schematic, exploded-view illustration of an SCV with constituent layers and components: silicone elastomer, battery, BLE SoC, Wheatstone bridge circuits configured with a 3D pressure sensor (R_P) and a temperature sensor (R_T), and circuit traces (copper/PI). (**B**) Circuit and block diagrams of the system and its wireless interface to smartphones. Analog front-end circuits consist of two differential AMPs and Wheatstone bridge circuits including resistive sensors (R_P and R_T) and reference resistors (R, R_{P0}, and R_{T0}). A central processing unit (CPU) transmits the ADC-sampled data (pressure/temperature measurements; V_P and V_T) via BLE radio to user interfaces (smartphones). (**C**) Photographs of SCV on the leg of a healthy patient (left) and with compression stocking (right). (**D**) Photograph of SCV during bending and twisting. (**E**) Computed strains along the copper traces and the components on the flexible printed circuit board (FPCB) in twisted (left) and bent (right) configurations. Photo credit: Yoonseok Park, Northwestern University.

agreement (Fig. 2B). The FEA results indicate that this compression induces a change in the maximum principal strain ($\varepsilon_{max\text{-}Au}$) of 0.26% for the metal trace on the 3D structure and a negligible change for the case of the 2D precursor (fig. S3).

Tests of the pressure response use wires attached with conductive epoxy (8331 Silver Adhesive; MG Chemicals) and mounted in a FPCB for electrical connection. A frame structure formed with acrylic and PI layers prevents excessive strains and minimizes the effects of shear stress (Fig. 2C and fig. S2C). Figure 2 (D and E) presents optical images and FEA results for compressive strains of 0, 12, and 24%, corresponding to pressures of 0, ~150, and ~300 mmHg. The experimental results agree with corresponding FEA predictions. The maximum principal strain across the gold trace ($\varepsilon_{max\text{-}Au}$) computed by FEA is 1.52% after assembly of 3D structure (fig. S4), which is below the fracture strain of gold, 10% (*34*, *35*). The changes in $\varepsilon_{max\text{-}Au}$ vary between 0.47 and 0.82% under 12 and 24% compression, respectively (Fig. 2D). In the target operating range (0 to 60 mmHg), $\Delta\varepsilon_{max\text{-}Au}$ is 0 to 0.19% (fig. S5), which is less than the yield threshold (0.3%). The changes in resistance correspond as expected with the degree of deformation (Fig. 2F).

Other parameters of interest are the linearity and the time scale of the response, as well as the long-term stability. Figure 3A shows results of tests of linearity, where the pressure follows from forces applied over controlled areas using a dynamic mechanical analysis (DMA; RSA-G2 Solids Analyzer, TA Instruments). A digital multimeter (NI-USB-4065, National Instrument) defines the change in resistance as the DMA records the applied force. The results indicate a high degree of linearity (R^2 = 0.992) and negligible hysteresis for pressures up to 120 mmHg. Furthermore, the response occurs within 200 ms, limited by the testing setup (in this measurement, the

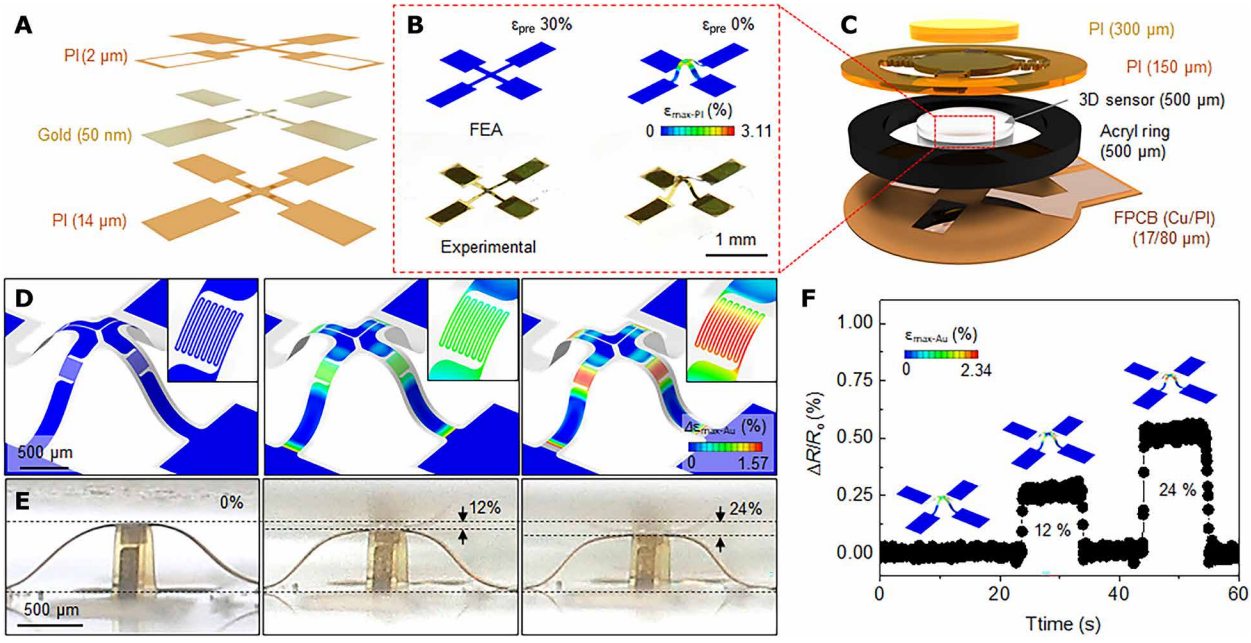

Fig. 2. Design and characterization of a 3D pressure sensor. (**A**) A tilted exploded view layout of the constituent layers of the 2D precursor consists of a top and bottom PI layer and gold layer (trace in a serpentine geometry; width, 3 μm; thickness, 50 nm; resistance, 2.1 kilohms). (**B**) Photographs and FEA-predicted results of a 2D precursor (left) and corresponding 3D structure (right) after a compressive buckling process. (**C**) Schematic exploded view illustration of a pressure sensor that consists of PI layers, acrylic ring, FPCB, and a 3D structure encapsulated in a transparent elastomer. FEA-predicted results and (inset) magnified view of changes in strain distributions across a metal strain gauge (**D**) and a photograph (**E**) of a 3D structure under compressive strain. (**F**) Change in resistance of a 3D structure under compressive strain (0, 12, and 24%), with insets that show FEA results. Photo credit: Yoonseok Park, Northwestern University.

sampling rate is 20 Hz), for both loading and unloading (Fig. 3B). The sensor exhibits good durability as well, with negligible variations in response over 1000 cycles under pressures of 50 mmHg (Fig. 3C). A circuit design similar to the one used for pressure sensing allows monitoring of temperature using a negative temperature coefficient (NTC) thermistor. The ADC value can be calibrated with a corresponding measurement of temperature using an infrared (IR) camera. The following equation determines the skin temperature (from 25°C) with an appropriate calibration factor

$$T = C_t(\mathrm{ADC_{NTC}} + n)$$

where $\mathrm{ADC_{NTC}}$ is the value from the ADC channel connected to the NTC and C_t and n are constants (table S1). Figure 3D shows good linearity in response (R^2 = 0.997), as compared to results obtained with an IR camera, for temperatures up to 45°C (fig. S6). Figure 3E shows an IR photograph of a sensor on the leg as a function of time. Thermal equilibration occurs within roughly 1 min at the top surface of the SCV; equilibration occurs on the bottom, near the location of the NTC, within tens of seconds (Fig. 3F).

Beyond the importance in monitoring the skin responses and wound healing processes, measurements of temperature are necessary to compensate changes in the responses of the pressure sensor that arise from changes in temperature (fig. S7). These temperature-dependent effects can be calibrated by applying pressures at different temperatures using the DMA. The calibration uses the following equation

$$P = C_{p1}(\mathrm{ADC_{pressure}} - C_{p2}(\mathrm{ADC_{NTC}} + m))$$

where $\mathrm{ADC_{pressure}}$ is the value from the ADC channel associated with the 3D pressure sensor and C_{p1}, C_{p2}, and m are calibration constants (table S1).

The performance of the SCV across different body types and tissue properties demands consistency in response across a range of curvatures and tissue modulus values. Systematic evaluations use flat and curved pieces of molded elastomers with different mechanical properties (Dragon Skin 10, E = 137 kPa; Ecoflex 00-50, E = 83 kPa; and Ecoflex 00-30, E = 69 kPa) with and without embedded stainless steel rods (diameter, 2.5 mm) to mimic the bone, as characteristic of the anatomy of the lower leg (fig. S8). The measured results indicate good agreement with values acquired using a commercial air bladder sensor (PicoPress) as a reference. The dimensions of the SCV (25 mm by 50 mm, 3.5 mm in thickness) are ~100 times smaller than the bladder device (160 mm by 90 mm, 30 mm in thickness), as shown in Fig. 4A. The tests involve use of the SCV and reference to determine the fractional change in pressure as a function of applied pressure for 11 different conditions (Fig. 4, B to D, and fig. S12A). All measured data up to 100 mmHg from the SCV show excellent agreement with applied pressure (mean difference of −1.26 mmHg and an SD of 2.74 mmHg) along with reference (mean difference of −4.13 mmHg and an SD of 1.90 mmHg; figs. S9 to S12).

To validate the operation on the skin, the SCV on the arm monitors fractional changes of pressure applied with a finger tip (movie S1) along with the interface pressure using a bandage. Movie S2 shows the change in applied pressure with the number of IBs wrapping on the arm. Figure 4E illustrates measurement sites on the leg for validation trials, including four sites at the C (maximum perimeter of

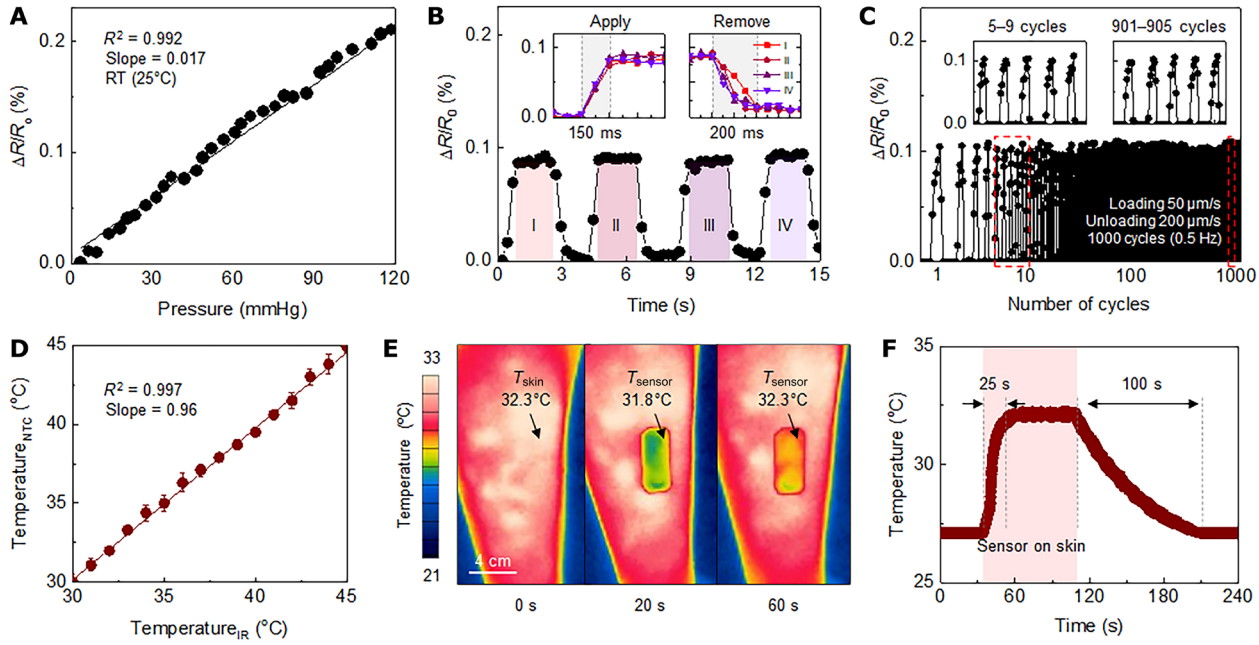

Fig. 3. Performance characteristics of a 3D pressure and temperature sensor. (**A**) Fractional change in resistance of a 3D pressure sensor as a function of normal pressure loading. RT, room temperature. (**B**) Measurement of the temporal response of a sensor and overlaid responses during applying and removing pressure (inset). (**C**) Fractional change of resistance at different stages of fatigue testing with a speed of 50 and 200 μm/s (loading and unloading) over 1000 cycles. (**D**) Response of an NTC temperature sensor as a function of temperature of a supporting substrate measured using an IR camera. (**E**) IR photograph of an SCV on the leg at two time points after mounting. (**F**) Temperature of the SCV before and after mounting on the skin and after removal.

the calf) and B_{m1} (manufacturer B_1; middle of B-C line, B; smallest perimeter of the leg) with a half π intervals at the axial location. The tests use the SCV and the reference to collect pressures at locations associated with two different grade compression stockings (SIGVARIS, 10 to 20 mmHg, 20 to 30 mmHg; SIGVARIS GROUP). The results in Fig. 4 (F and G) indicate that the reference pressures are ~25% higher on bony locations (C_1 and B_{m5}) than other locations, likely because of effects of bending caused by the relatively large size of the air bladder compared to the bending radius at C_1 (~30 mm). By contrast, the miniature dimensions of the SCV lead to relatively consistent readings across all locations (SDs of 1.85 and 1.65 mmHg, respectively, with 10 to 20 mmHg and 20 to 30 mmHg GCS) compared to those of the reference (SDs of 2.58 and 3.09 mmHg, respectively, with 10 to 20 mmHg and 20 to 30 mmHg GCS). When wearing a GCS with SCV on the leg (fig. S13), effects of motion are visible in the data, with possible relevance to characterization of gait and gait-induced changes in pressure. Results from an SCV and a reference bonded to C_2 evaluated under sitting, walking, running, and cycling conditions appear in Fig. 4 (H to G). As might be expected, stable readings occur during sitting, and fluctuations arise from the SCV (mean, 28.7 mmHg; SD, 0.316 mmHg) from small movements (Fig. 4H). The readings obtained with the reference show constant values of 28 mmHg since the pressures display in increments of 1 mmHg. Walking and running induce large variations with both sensors ($P_{peak\text{-}to\text{-}peak}$; 2 mmHg in reference and 1.1 mmHg in SCV; Fig. 4I). Cycling shows relatively small variations (Fig. 4G).

Tests to evaluate applicability for use during normal daily life involve monitoring for 6 hours with the SCV at location C_2 while wearing a GCS set for a pressure of 20 to 30 mmHg. Figure 5 (A to D) shows the measured pressure and temperature values during sitting in front of a desk, sleeping, cycling and while walking indoors and outdoors. The pressure changes depend on the activities as described above, and the temperature varies both with the ambient temperature and the skin temperature, with noted increases during physical exercise. FEA results indicate that the soft, encapsulated thin and miniaturized SCV induces negligible additional load on the skin (fig. S14). After 6 hours with the SCV while wearing a GCS, a slightly pressed mark can be observed on the skin which recovers over 20 min (fig. S15). These results suggest the potential for the SCV to monitor pressure applied through the GCS to the legs of patients with VLU and simultaneously to measure skin temperature in the vicinity of an ulcer to track healing.

Clinical studies involve older adult patients with a history of venous insufficiency, VLUs, or deep vein thromboses (table S2). SCV and reference equipment mount at two points (C_1 and C_3, Fig. 6A; C_2 and C_4, Fig. 6B) on the left and right legs of each patient wearing GCS (SIGVARIS, 20 to 30 mmHg; SIGVARIS GROUP) based on their ankle and calf circumference. Use of the GCS directly for purposes of validating the performance of the system avoids inconsistencies in pressures delivered by a sphygmomanometer for example (*36*). The pressure at each location shows some individual variability. Averaged pressures across each leg measured by clinical studies serve as points of comparison. The pressures measured at the locations C_2 and C_4 show good agreement between the reference and SCV with six patients (patient numbers 1 to 6; Fig. 6B) along with C_1 and C_3 with three patients (patient numbers 2, 7, and 8; Fig. 6D). Measurements on the patient with varicose veins (Fig. 6, E and F) show excellent agreement between reference and SCV at each location. During a month of clinical study, the VLUs on the left leg of the patient recover within 3 weeks and the pressures

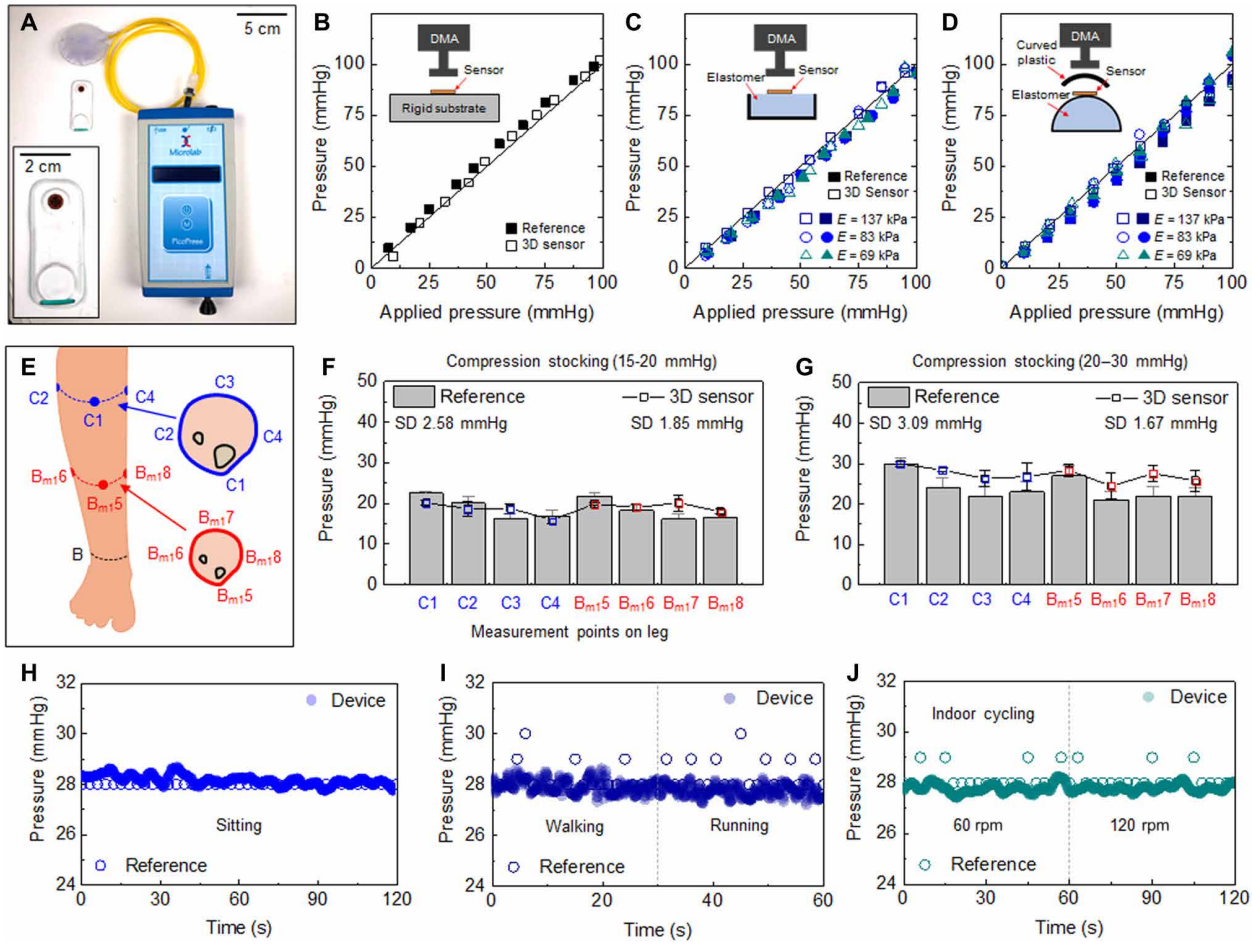

Fig. 4. Evaluations of a wireless 3D pressure sensor and a reference device performed with a DMA and with a compression stocking mounted on the legs of healthy volunteers. (**A**) Photograph of a wireless sensor and a reference sensor (PicoPress, Microlab) of pressure. Changes in the resistance of the 3D sensor and response of the reference equipment as a function of pressure on a (**B**) flat rigid surface, (**C**) flat elastic surface, and (**D**) curved elastic surface with different materials [elastomers with different elastic modulus; Dragon Skin 10 (E = 137 kPa), Ecoflex 00-50 (E = 83 kPa), and Ecoflex 00-30 (E = 69 kPa)]. (**E**) Schematic illustration of eight measurement points across the leg. Measured changes in pressure and resistance on the leg of a healthy volunteer using a compression stocking at pressures of (**F**) 15 to 20 mmHg and (**G**) 20 to 30 mmHg. Pressure measurement using the SCV and the reference equipment during (**H**) resting, (**I**) walking and running, and (**J**) cycling with speeds of 60 and 120 rpm. Photo credit: Yoonseok Park, Northwestern University.

measured every week using reference and SCV devices exhibit good agreement (Fig. 6, G and H). This result provides evidence of the accurate measurement of interface pressure by SCV in the process of recovery from ulcers. The Bland-Altman plot in Fig. 6I shows that the SCV performs well regardless of leg characteristics according to various diseases and ages.

DISCUSSION

The flexible, lightweight, wireless platforms introduced in this study support simultaneous monitoring of pressures and temperatures at the interfaces between compressive garments and the skin. A mechanically guided 3D assembly approach yields soft pressure sensors that exhibit high linearity and negligible hysteresis across the entire range of pressures relevant for this application. Experimental studies and trials on healthy subjects demonstrate accurate, stable monitoring performance, with quantitative accuracy as determined through comparison to reference devices. Clinical studies with patients that exhibit different pathologies illustrate capabilities for measuring pressures for different body types and skin conditions. Specific demonstrations in various practical scenarios highlight continuous tracking while sleeping, walking, and cycling. The core technology has clear potential for use not only in the clinic but also in the home, for improved health outcomes by enabling the precise measurement and necessary adjustment of therapeutic pressure delivered by GCS. Additional options include direct integration of this type of low-profile sensor with existing GCS products as instrumented "smart" stockings.

MATERIALS AND METHODS

Fabrication of the 3D pressure sensor

Preparation of 2D precursors began with spin coating (3000 rpm for 30 s) and curing (180°C for 2 min) a thin layer of poly(methyl methacrylate) (PMMA) on a clean glass slide, followed by spin coating and fully curing (260°C for 1 hour) a layer of PI (14 μm;

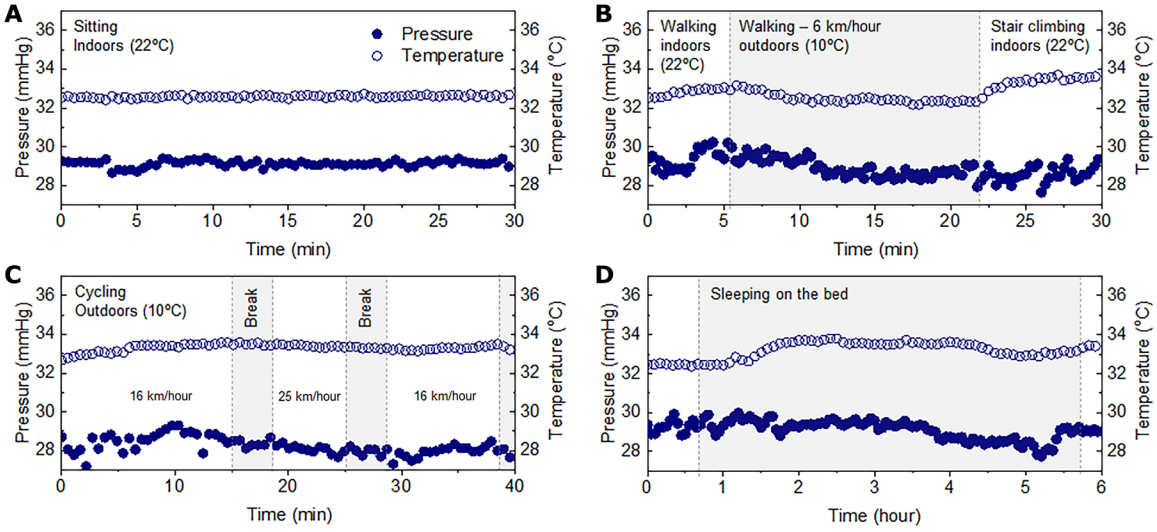

Fig. 5. Pressure and temperature measurements obtained using a wireless 3D pressure/temperature sensor during daily activities with a compression stocking. Pressure and temperature measurements while (**A**) in a sitting position, (**B**) walking indoors and outdoors, (**C**) cycling at a self-selected low (16 km/hour) and high (25 km/hour) speed, and (**D**) sleeping for 6 hours.

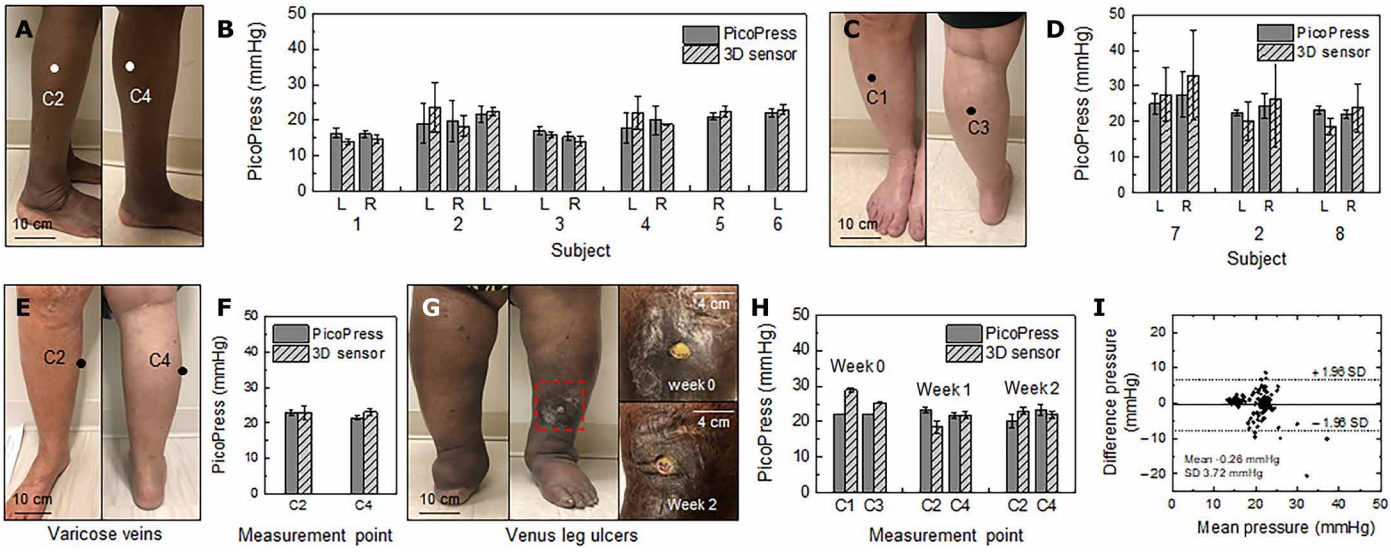

Fig. 6. Clinical studies of interface pressure measured by SCV and reference devices from eight patients with different pathologies. Photographs of measurement locations on the leg of a patient and pressures measured by SCV and reference devices at locations C_2 and C_4 (**A** and **B**) and C_1 and C_3 (**C** and **D**) on the left (L) and right (R) legs of patients using compression stockings. Photographs of the right leg and changes in pressure of a patient with varicose veins (**E** and **F**). (**G**) Photographs of the left leg and the VLU of a patient and measured pressures for 2 weeks (**H**). (**I**) Bland-Altman plot comparing results from the SCV and reference devices. Photo credit: Brianna R. Kampmeier, Northwestern University.

PI-2545, HD MicroSystems). Electron beam evaporation formed thin films of chrome (Cr, 5 nm) and gold (Au, 50 nm) on the PI. Photolithography and lift-off yielded serpentine patterns in these thin metal films. Spin coating and curing another layer of PI (2 μm) created an insulating film on these conductive features. A thin layer of copper (Cu, 50 nm) deposited on the PI by sputtering and patterned by photolithography and wet etching served as a hard mask for oxygen plasma etching (220 mT, 200 W, 120 min) of the exposed regions of the PI. Immersion in acetone overnight dissolved the underlying PMMA, thereby allowing the structures to be retrieved from the glass slide. Transferring this 2D precursor onto the surface of a poly(dimethylsiloxane) stamp and again onto the surface of a water-soluble tape prepared the system for the buckling process. We prestretched an elastomer substrate to an equal biaxial strain of 30% and laminated the 2D precursors/Poly(vinyl alcohol) tape on top. Van der Waals force associated with contact of the 2D precursor (PI) to the elastomer substrate (Dragon Skin, Smooth-On, PA, USA), the rectangular-shaped contact area (1.4 mm by 0.8 mm), has larger area and, accordingly, higher bonding energy than the narrow ribbon-shaped area (0.18 mm by 0.8 mm). Dissolving the PVA

tape with water and releasing the prestrain transformed the 2D precursors into 3D mesostructures, while rectangular-shaped contact area acts as a bonding site. Encapsulating the 3D structure in Ecoflex 00-30 (Smooth-On, PA, USA) using a mold (diameter, 3 mm; height, 500 μm) completed the fabrication process. Placing the encapsulated 3D structures on an FPCB allowed for electrical interconnection using a conductive epoxy. A ring-shaped structure of acrylic and PI layers stacked on the 3D sensor provided mechanical stability. Illustrations in fig. S1 feature each step in detail.

Fabrication of the electronics

FPCB design layouts used EAGLE CAD version 9 (Autodesk). Fabrication began with patterning a sheet of FPCB (12-μm-thick top and bottom Cu layer, 25-μm-thick middle PI layer; AP7164R, DuPont) into the necessary shapes using an ultraviolet laser cutter (LPKF U4). Solder paste (Chip Quik TS391LT) joined the 3D pressure sensor and the various surface-mount components including BLE SoC (nRF52832, Nordic Semiconductor), BLE antenna (2450AT18A100, Johanson Technology Inc.), AMP (INA333, Texas Instruments), reference resistors (RMCF0201FT, Stackpole Electronics Inc.), and temperature sensor components (NTC; NCP03XH, Murata) onto the FPCB by reflow using a heat gun (AOYUE Int866). The temperature sensor components provided high accuracy in resistance and long-term stability.

Assembly of the wireless device

A film of a soft silicone material (SILBIONE RTV 4420; A&B, Bluestar Silicones) formed by spin-casting at 250 rpm and thermal curing (100°C in an oven for 20 min) on a glass slide served as the bottom layer for the encapsulation process. A milling machine (Roland MDX-540) created aluminum molds in geometries defined by 3D computer-aided design drawings created using SOLIDWORKS 2020. The capping membrane was defined by casting a liquid precursor to a silicone polymer (SILBIONE RTV 4420; A&B, Bluestar Silicones) and thermal curing in an oven at 100°C for 20 min. A cutting process with a CO_2 laser (Universal Laser Systems, Inc.) defined an opening for the pressure sensor and a replaceable battery on the capping layer. A manual process aligned openings on the capping layer to the pressure sensor and battery on FPCB.

Characterizing the pressure sensor

A DMA and compression stockings mounted on the legs of study subjects allowed for comparisons between measurements with the 3D sensor and the reference device. Changes in resistance and calibrated pressure readings from the 3D sensor as a function of pressure applied using a dynamic mechanical analyzer (RSA-G2 Solids Analyzer, TA Instruments) were stored through wireless communication. Pressures displayed on PicoPress (reference) were manually recorded.

Feasibility tests of the wireless device

The studies involved a volunteer (male, 39 years old) with a pressure sensor placed on the leg at eight locations including four sites at the C (max perimeter of the calf) and B_{m1} (manufacturer B_1; middle of B-C line, B; smallest perimeter of the leg) with half π intervals at the axial position. The volunteer sat at a desk, and pressures were measured at each location with PicoPress and SCV. The same volunteer performed various activities (walking, cycling indoor and outdoor, and sleeping) with the SCV at C_2.

Characterizing the temperature sensor

Measurements of the accuracy of the temperature sensor involved placing the SCV on a hotplate, heating to 42°C, and then cooling to room temperature, with simultaneous measurements using an IR camera (FLIR) as a standard.

Finite element analysis

The commercial software suite Abaqus was used to design the 3D structure and the wireless device and to optimize their mechanical performance. Four-node shell elements were used for the PI thin films and metal (gold and copper) traces, and eight-node solid elements were used for the silicone materials. Mesh convergence was tested for all computational cases. PI was modeled as a linear elastic material with an elastic modulus of E_{PI} = 2.5 GPa and a Poisson's ratio of ν_{PI} = 0.34. Metals materials (gold and copper) were modeled as elastoplastic (without hardening; yield strain chosen as 0.3%). The elastic modulus (E) and Poisson's ratio (ν) are E_{Au} = 79 GPa and ν_{Au} = 0.4 for gold (Au) and E_{Cu} = 119 GPa and ν_{Cu} = 0.34 for copper (Cu), respectively. The Ecoflex 00-30 silicone material was modeled as an incompressible Mooney-Rivlin solid with an elastic modulus of $E_{Ecoflex}$ = 60 kPa.

Clinical studies

This study was approved by the Northwestern University's Institutional Review Board, under trial registration number STU00206331-CR0002. After informed consent for all participants, participants wore compressive garments on their left and right legs. The SCV and reference equipment (PicoPress) were placed on the calf by trained research staff, and applied interface pressures through GCS were recorded.

SUPPLEMENTARY MATERIALS

Supplementary material for this article is available at http://advances.sciencemag.org/cgi/content/full/6/49/eabe1655/DC1

View/request a protocol for this paper from *Bio-protocol*.

REFERENCES AND NOTES

1. C. S. Lim, A. H. Davies, Graduated compression stockings. *CMAJ.* **186**, E391–E398 (2014).
2. C. K. Sen, G. M. Gordillo, S. Roy, R. Kirsner, L. Lambert, T. K. Hunt, F. Gottrup, G. C. Gurtner, M. T. Longaker, Human skin wounds: A major and snowballing threat to public health and the economy. *Wound Repair Regen.* **17**, 763–771 (2009).
3. J. M. Gelfand, O. Hoffstad, D. J. Margolis, Surrogate endpoints for the treatment of venous leg ulcers. *J. Invest. Dermatol.* **119**, 1420–1425 (2002).
4. E. N. Mostow, G. D. Haraway, M. Dalsing, J. P. Hodde, D. King; OASIS Venus Ulcer Study Group, Effectiveness of an extracellular matrix graft (OASIS Wound Matrix) in the treatment of chronic leg ulcers: A randomized clinical trial. *J. Vasc. Surg.* **41**, 837–843 (2005).
5. Apligraf, Organogenesis Inc. (2012); https://organogenesis.com/advanced-wound-care/apligraf/product-information.html.
6. M. B. Malas, U. Qazi, G. Lazarus, M. F. Valle, L. M. Wilson, E. B. Haberl, E. B. Bass, J. Zenilman, Comparative effectiveness of surgical interventions aimed at treating underlying venous pathology in patients with chronic venous ulcer. *J. Vasc. Surg. Venous Lymphat. Disord.* **2**, 212–225 (2014).
7. E. Foy White-Chu, T. A. Conner-Kerr, Overview of guidelines for the prevention and treatment of venous leg ulcers: A US perspective. *J. Multidiscip. Healthc.* **7**, 111–117 (2014).
8. S. D. Blair, D. D. Wright, C. M. Backhouse, E. Riddle, C. N. McCollum, Sustained compression and healing of chronic venous ulcers. *BMJ* **297**, 1159–1161 (1988).
9. W. A. Marston, R. E. Carlin, M. A. Passman, M. A. Farber, B. A. Keagy, Healing rates and cost efficacy of outpatient compression treatment for leg ulcers associated with venous insufficiency. *J. Vasc. Surg.* **30**, 491–498 (1999).
10. C. Moffatt, D. Kommala, N. Dourdin, Y. Choe, Venous leg ulcers: Patient concordance with compression therapy and its impact on healing and prevention of recurrence. *Int. Wound J.* **6**, 386–393 (2009).

11. E. Rabe, H. Partsch, J. Hafner, C. Lattimer, G. Mosti, M. Neumann, T. Urbanek, M. Huebner, S. Gaillard, P. Carpentier, Indications for medical compression stockings in venous and lymphatic disorders: An evidence-based consensus statement. *Phlebology* **33**, 163–184 (2018).
12. Y.-W. Chi, K.-H. Tseng, R. Li, T. Pan, Comparison of piezoresistive sensor to PicoPress in in-vitro interface pressure measurement. *Phlebology* **33**, 315–320 (2018).
13. Small Force Sensing Resistor, FlexiForce A301 Sensor, Tekscan; www.tekscan.com/products-solutions/force-sensors/a301.
14. Half Inch ThruMode FSR; www.sensitronics.com/products-half-inch-thru-mode-fsr.php.
15. Interlink Sensor Technologies; www.interlinkelectronics.com/sensor-technologies.
16. F. Amsler, T. Willenberg, W. Blättler, In search of optimal compression therapy for venous leg ulcers: A meta-analysis of studies comparing divers bandages with specifically designed stockings. *J. Vasc. Surg.* **50**, 668–674 (2009).
17. R. J. Damstra, E. R. Brouwer, H. Partsch, Controlled, comparative study of relation between volume changes and interface pressure under short-stretch bandages in leg lymphedema patients. *Dermatol. Surg.* **34**, 773–778 (2008).
18. M. M. Heinen, C. van der Vleuten, M. J. M. de Rooij, C. J. T. Uden, A. W. M. Evers, T. van Achterberg, Physical activity and adherence to compression therapy in patients with venous leg ulcers. *Arch. Dermatol.* **143**, 1283–1288 (2007).
19. J. Li, L. Fang, B. Sun, X. Li, S. H. Kang, Review—Recent progress in flexible and stretchable piezoresistive sensors and their applications. *J. Electrochem. Soc.* **167**, 037561 (2020).
20. G. Ge, Y. Cai, Q. Dong, Y. Zhang, J. Shao, W. Huang, X. Dong, A flexible pressure sensor based on rGO/polyaniline wrapped sponge with tunable sensitivity for human motion detection. *Nanoscale* **10**, 10033–10040 (2018).
21. L. Pan, A. Chortos, G. Yu, Y. Wang, S. Isaacson, R. Allen, Y. Shi, R. Dauskardt, Z. Bao, An ultra-sensitive resistive pressure sensor based on hollow-sphere microstructure induced elasticity in conducting polymer film. *Nat. Commun.* **5**, 3002 (2014).
22. N. Matsuhisa, D. Inoue, P. Zalar, H. Jin, Y. Matsuba, A. Itoh, T. Yokota, D. Hashizume, T. Someya, Printable elastic conductors by *in situ* formation of silver nanoparticles from silver flakes. *Nat. Mater.* **16**, 834–840 (2017).
23. Z. Lou, S. Chen, L. Wang, K. Jiang, G. Shen, An ultra-sensitive and rapid response speed graphene pressure sensors for electronic skin and health monitoring. *Nano Energy* **23**, 7–14 (2016).
24. H.-B. Yao, J. Ge, C.-F. Wang, X. Wang, W. Hu, Z.-J. Zheng, Y. Ni, S.-H. Yu, A flexible and highly pressure-sensitive graphene-polyurethane sponge based on fractured microstructure design. *Adv. Mater.* **25**, 6692–6698 (2013).
25. H.-H. Chou, A. Nguyen, A. Chortos, J. W. F. To, C. Lu, J. Mei, T. Kurosawa, W.-G. Bae, J. B.-H. Tok, Z. Bao, A chameleon-inspired stretchable electronic skin with interactive colour changing controlled by tactile sensing. *Nat. Commun.* **6**, 8011 (2015).
26. Y. Cao, T. Li, Y. Gu, H. Luo, S. Wang, T. Zhang, Fingerprint-inspired flexible tactile sensor for accurately discerning surface texture. *Small* **14**, 1703902 (2018).
27. G. Schwartz, B. C.-K. Tee, J. Mei, A. L. Appleton, D. H. Kim, H. Wang, Z. Bao, Flexible polymer transistors with high pressure sensitivity for application in electronic skin and health monitoring. *Nat. Commun.* **4**, 1859 (2013).
28. J. W. Boley, E. L. White, R. K. Kramer, Mechanically sintered gallium-indium nanoparticles. *Adv. Mater.* **27**, 2355–2360 (2015).
29. Y.-L. Park, B.-R. Chen, R. J. Wood, Design and fabrication of soft artificial skin using embedded microchannels and liquid conductors. *IEEE Sens. J.* **12**, 2711–2718 (2012).
30. S. Xu, Z. Yan, K.-I. Jang, W. Huang, H. Fu, J. Kim, Z. Wei, M. Flavin, J. M. Cracken, R. Wang, A. Badea, Y. Liu, D. Xiao, G. Zhou, J. Lee, H. U. Chung, H. Cheng, W. Ren, A. Banks, X. Li, U. Paik, R. G. Nuzzo, Y. Huang, Y. Zhang, J. A. Rogers, Assembly of micro/nanomaterials into complex, three-dimensional a by compressive buckling. *Science* **347**, 154–159 (2015).
31. Y. Park, H. Luan, K. Kwon, S. Zhao, D. Franklin, H. Wang, H. Zhao, W. Bai, J. U. Kim, W. Lu, J.-H. Kim, Y. Huang, Y. Zhang, J. A. Rogers, Transformable, freestanding 3D mesostructures based on transient materials and mechanical interlocking. *Adv. Funct. Mater.* **29**, 1903181 (2019).
32. S. M. Won, H. Wang, B. H. Kim, K. H. Lee, H. Jang, K. Kwon, M. Han, K. E. Crawford, H. Li, Y. Lee, X. Yuan, S. B. Kim, Y. S. Oh, W. J. Jang, J. Y. Lee, S. Han, J. Kim, X. Wang, Z. Xie, Y. Zhang, Y. Huang, J. A. Rogers, Multimodal sensing with a three-dimensional piezoresistive structure. *ACS Nano* **13**, 10972–10979 (2019).
33. J. W. Kwak, M. Han, Z. Xie, H. U. Chung, J. Y. Lee, R. Avila, J. Yohay, X. Chen, C. Liang, M. Patel, I. Jung, K. Jongwon, M. Namkoong, K. Kwon, X. Guo, C. Ogle, D. Grande, D. Ryu, D. H. Kim, S. Madhvapathy, C. Liu, D. S. Yang, Y. Park, R. Caldwell, A. Bank, S. Xu, Y. Huang, S. Fatone, J. A. Rogers, Soft, wireless electronic system for continuous, multimodal measurements of physiological health at the skin interface with prostheses.
34. H. Hocheng, C.-M. Chen, Design, fabrication and failure analysis of stretchable electrical routings. *Sensors.* **14**, 11855–11877 (2014).
35. K.-I. Jang, Y. Ma, A. Koh, H. Chen, H. N. Jung, Y. Kim, J. W. Kwak, L. Wang, Y. Xue, Y. Yang, W. Tian, Y. Jiang, Y. Zhang, X. Feng, Y. Huang, J. A. Rogers, Chemical sensing systems that utilize soft electronics on thin elastomeric substrates with open cellular designs. *Adv. Funct. Mater.* **27**, 1605476 (2017).
36. I. Jung, Z. Xie, Q. Huo, J. Kim, J. Lee, B. Ji, S. Xu, *In vitro* protocol for validating interface pressure sensors for therapeutic compression garments: Importance of sphygmomanometer placement and initial cuff diameter. *Veins Lymphat.* **7**, 7204 (2018).

Acknowledgments

Funding: The materials and engineering efforts were supported by the Querrey-Simpson Institute for Bioelectronics. This work made use of the NUFAB facility of Northwestern University's NUANCE Center, which has received support from the Soft and Hybrid Nanotechnology Experimental (SHyNE) Resource (NSF ECCS-1542205); the MRSEC program (NSF DMR-1720139) at the Materials Research Center; the International Institute for Nanotechnology (IIN); the Keck Foundation; and the State of Illinois, through the IIN. Y.P. acknowledges the support from the German Research Foundation, Germany (PA 3154/1-1). S.M.W. acknowledges the support from the MSIT(Ministry of Science and ICT) Korea, under the ICT Creative Consilience program (IITP-2020-0-01821) supervised by the IITP (Institute for Information & Communications Technology Planning & Evaluation). Y.H. acknowledges the support from the NSF, USA (CMMI1635443). S.X. and J.A.R. acknowledge the support from the NIH, USA (1R43AG059445-01). **Author contributions:** Y.P., K.K., S.X., and J.A.R. conceived the overall research goals and aims. Y.P. and J.A.R. performed the designs and engineering investigation of the sensor. Y.P., K.K., S.S.K., D.S.Y., T.S.C., J.U.K., H. Jang, H.R., H. Jeong, S.M.W., Y.J.K., and S.H.S. manufactured the sensors and wireless devices. K.K. and S.S.K. designed the hardware for the wireless electronics platform. K.K. and K.S.C. performed software design and software validation. H.L., I.J., and Y.H. performed mechanical modeling. Y.P., D.S.Y., and J.W.K. performed in vitro characterizations. B.R.K., M.Z., D.P., J.Z., and S.X. recruited participants. Y.P., B.R.K., M.Z., D.P., and S.X. performed clinical data collection and analysis. Y.P., K.K., and J.A.R. were responsible for original drafting of the manuscript, and all authors assisted in critical editing and review of the final manuscript. **Competing interests:** J.A.R. and S.X. are unpaid cofounders of a company that may explore commercial applications of this technology. The other authors declare that they have no competing interests. **Data and materials availability:** All data needed to evaluate the conclusions in the paper are present in the paper and/or the Supplementary Materials. Additional data related to this paper may be requested from the authors.

Submitted 4 August 2020
Accepted 20 October 2020
Published 4 December 2020
10.1126/sciadv.abe1655

Citation: Y. Park, K. Kwon, S. S. Kwak, D. S. Yang, J. W. Kwak, H. Luan, T. S. Chung, K. S. Chun, J. U. Kim, H. Jang, H. Ryu, H. Jeong, S. M. Won, Y. J. Kang, M. Zhang, D. Pontes, B. R. Kampmeier, S. H. Seo, J. Zhao, I. Jung, Y. Huang, S. Xu, J. A. Rogers, Wireless, skin-interfaced sensors for compression therapy. *Sci. Adv.* **6**, eabe1655 (2020).